A Data-Driven Multiscale Theory for Modeling Damage and Fracture of Composite Materials

Modesar Shakoor, Jiaying Gao, Zeliang Liu, Wing Kam Liu

A Data-Driven Multiscale Theory For Modeling Damage and Fracture of Heterogeneous Materials

Modesar Shakoor, Jiaying Gao, Zeliang Liu, and Wing Kam Liu

Abstract The advent of advanced processing and manufacturing techniques has led to new material classes with complex microstructures across scales from nanometers to meters. In this paper, a data-driven multiscale theory for the analysis of these complex material systems is presented. A mechanistic concurrent multiscale method called Self-consistent Clustering Analysis (SCA) is developed for general inelastic heterogeneous material systems. The efficiency of SCA is achieved via data compression algorithms which group local microstructures into clusters during the training stage, thereby reducing required computational expense. Its accuracy is guaranteed by introducing a self-consistent method for solving the Lippmann-Schwinger integral equation in the prediction stage. The proposed theory is illustrated for a composite cutting process where fracture can be analyzed simultaneously at the microstructure and part scales.

1 Introduction

The analysis and design of new materials with improved efficiency and performance requires cutting edge process and material modeling theories. For instance, new lightweight vehicles are being developed using lighter material systems [7]. Conventional processing-structure-property-performance relationships must be reconsidered to account for the microstructural complexity of new advanced materials systems such as hierarchical materials [15]. In this

Modesar Shakoor · Jiaying Gao · Wing Kam Liu
Department of Mechanical Engineering, Northwestern University, Evanston, IL, USA
e-mail: w-liu@northwestern.edu

Zeliang Liu
Livermore Software Technology Corporation (LSTC), Livermore, CA 94551, USA

aim, integrated computational materials engineering approaches relying on predictive multiscale modeling theories are being developed [12, 16].

In this paper, a data-driven multiscale modeling theory is presented and applied to a problem involving a process-structure relationship. This relationship emerges from microstructure modeling using computational homogenization and reduced order modeling.

The first novelty of the proposed data-driven multiscale modeling theory is the use of the so-called Self-consistent Clustering Analysis (SCA) [9]. This method relies on the Fast Fourier Transform (FFT) based numerical method introduced in Ref. [14], which formulates conventional balance equations with periodic boundary conditions as a periodic Lippmann-Schwinger equation. The originality in SCA is that the Lippmann-Schwinger equation is solved using a clustered discretization. The voxel mesh Direct Numerical Simulation (DNS) model of the microstructure is hence reduced into clusters of voxels, and degrees of freedom in the reduced model are defined cluster-wise instead of voxel-wise. This reduces mesh dependency in the RVE due to the built-in local averaging characteristics of the clusters.

Voxels clustering is performed using the k-means clustering method [11] applied on a database of DNS results for the studied microstructure. These DNS results do not need to include complex loading paths, as accurate predictions could be obtained in a previous work using only proportional loading paths in 6 orthogonal directions [9]. In fact, in this previous work DNS results were obtained using small strain amplitudes for which material response remained in the linear elastic range.

The second novelty of the proposed data-driven multiscale modeling theory is its capability to model damage and fracture at multiple scales [10]. A concurrent computational homogenization scheme is developed in order to solve any macroscale problem with material laws computed on the fly from microstructure information. In this scheme, the macroscale problem is solved using the FE method, with the particularity that conventional phenomenological constitutive equations are replaced by micromechanical problems solved using SCA. These micromechanical models, called Representative Volume Elements (RVEs), include enough microstructural features to be statistically representative of the local microstructure around each material integration point. Moreover, the RVEs are solved by SCA, which defines non-local interaction tensors among material clusters and can be considered as a specific type of meshfree method. This nonlocal effect introduced by SCA also avoids localization issues at RVE scale.

Damage modeling leads to well-known localization and pathological mesh dependence issues. In the context of concurrent computational homogenization, these issues arise at two scales. Indeed, pathological localization can occur within arbitrary elements of the macroscale problem discretization, and also within arbitrary clusters of microscale problems discretizations. In the

proposed data-driven multiscale damage modeling theory [10], the damage variable is regularized at the macroscale using non local integral averaging to avoid any localization between RVEs, while at the microscale it is coupled to constitutive equations in an average sense to avoid any localization within RVEs.

The paper is structured as follows. It starts with a presentation of SCA in Sect. 2, followed by details on its exploitation for multiscale damage modeling in Sect. 3. The relevance of the proposed data-driven multiscale modeling theory is illustrated by applications in Sect. 4.

A multiscale simulation of the cutting of a Unidirectional (UD) Carbon Fiber Reinforced Polymer (CFRP) composite is conducted to show how fracture can be modeled simultaneously at two scales with the proposed theory.

2 Self-consistent Clustering Analysis

In the Finite Element (FE) method, the displacement field is discretized at mesh nodes, and material integration is conducted at integration points. Reducing the number of displacement degrees of freedom does not directly reduce neither the number of integration points nor the cost of material integration. Therefore, FE based model order reduction methods must be coupled to material integration reduction techniques in order to be efficiently applicable to nonlinear materials [3, 4, 5].

In the FFT-based numerical method [14], the strain field is discretized voxel-wise, and material integration is conducted voxel-wise as well. As a consequence, reducing the number of strain degrees of freedom directly reduces the cost of both Lippmann-Schwinger equation solution and material integration. In comparison to FE based model order reduction methods [3, 4, 5], SCA is hence a more straightforward approach to reduced order modeling [9]. This approach is briefly summarized in the following. The reader is referred to Ref. [9] for a full description, and to Ref. [17] for discussions on mathematical foundations. Details on the clustering algorithm can be found in Ref. [11].

In the following, the superscript ^{m} indicates microscale variables that are discretized voxel-wise in the FFT-based numerical method, and cluster-wise in SCA. The RVE domain over which Eq. (2) is solved is denoted Ω^m. The superscript ^{M} indicates macroscopic variables that are homogeneous over the RVE.

2.1 Continuous Lippmann-Schwinger equation

First order homogenization consists in defining the infinitesimal strain tensor field in the RVE ε^m as the addition of the macroscopic (homogeneous) strain ε^M and a microscopic (heterogeneous) fluctuation. As proved in Ref. [14], Hill's lemma enables to define the macroscopic Cauchy stress tensor σ^M as the average of the microscopic one $\sigma^M = \frac{1}{|\Omega^m|}\int_{\Omega^m}\sigma^m(\mathrm{x})\mathrm{dx}$.

Hill's lemma requires $(\varepsilon^m - \varepsilon^M)$ to verify compatibility, *i.e.*, to derive from a periodic displacement field, and σ^m to verify equilibrium, *i.e.* to be the solution of

$$\nabla.\sigma^m(\mathrm{x}) = 0, \mathrm{x} \in \Omega^m. \tag{1}$$

As shown in Ref. [17], Eq. (1) is equivalent to

$$\varepsilon^m(\mathrm{x}) = -\int_{\Omega^m} \Phi^0(\mathrm{x},\mathrm{x}') : \left(\sigma^m(\mathrm{x}') - \mathrm{C}^0 : \varepsilon^m(\mathrm{x}')\right)\mathrm{dx}' + \varepsilon^0, \mathrm{x} \in \Omega^m. \tag{2}$$

Eq. (2) is the Lippmann-Schwinger equation for first order homogenization. The fourth rank tensor C^0 is the stiffness tensor associated to an isotropic linear elastic reference material. This tensor will be determined in Sect. 2.2.2, as well as the far field strain tensor ε^0 and the periodic Green's operator Φ^0. The latter maps any tensor field τ^m to a compatible one:

$$\exists u \in (H^1(\Omega^m))^3, u \text{ periodic on } \Omega^m, -\Phi^0 * \tau^m = \frac{1}{2}(\nabla u + \nabla u^T). \tag{3}$$

The combination of Eqs. (2) and (3) yields a microscopic infinitesimal strain tensor ε^m that verifies compatibility and a Cauchy stress tensor σ^m that verifies equilibrium.

2.2 Discrete Lippmann-Schwinger equation

SCA consists in solving Eq. (2) cluster-wise instead of voxel-wise. Fig. 1a shows an example of voxel mesh for a single inclusion embedded within a matrix material. This voxel mesh is clustered in Fig. 1b. The clustering method for the training stage is presented in Sect. 2.2.1, including the construction of the database of DNS results. The use of this database to compute the mechanical response by solving the discrete Lippmann-Schwinger equation in the prediction stage is described in Sect. 2.2.2.

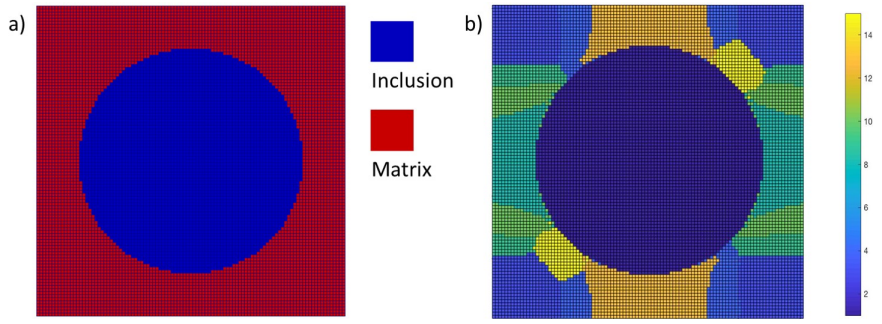

Fig. 1 Example of microstructure discretized using: (a) voxels; (b) clusters

2.2.1 Training stage

The aim of the training stage is to compute a cluster-wise discretization such as shown in Fig. 1. The mechanical response obtained by solving the Lippmann-Schwinger equation discretized cluster-wise should be as close as possible as that obtained by solving it voxel-wise. This can be done *a posteriori*, by solving the reduced order model for different trial configurations of clusters and searching for the optimal one. It can also be done *a priori*, for instance by basing the clustering algorithm on some mechanistic criterion such as the similarity in strain concentration tensors [9]. The strain concentration tensor field A^m is the fourth order tensor field defined by

$$\varepsilon^m(\mathrm{x}) = A^m(\mathrm{x}) : \varepsilon^M, \mathrm{x} \in \Omega^m. \tag{4}$$

At a given instant T, the strain concentration tensor field depends on the applied macroscopic strain ε^M and, for plastic materials, on the loading history $\left(\varepsilon_t^M\right)_{t \leq T}$. It is neither possible to compute the A^m fields for all potential loading paths, nor is it possible to apply clustering directly to data of such high dimensionality. Therefore, the space of all possible A^m fields must be sampled down to a few loading paths [4]. As shown in a previous study [9], the most cost-efficient way to do this sampling in the case of SCA is to consider only very small macroscopic strains ε^M in the training stage. For such strains, the mechanical response is purely elastic and linear, and the single tensor field A^m, which has only 36 independent components due to symmetries of ε^m and ε^M, can be computed by conducting 6 DNS in 6 orthogonal loading directions.

The training data set hence consists in 36 values for each voxel of the DNS mesh. A k-means clustering algorithm [11] is applied to this data set. Since the microstructure is a heterogeneous domain composed of multiple phases, clustering is done independently for each of those phases, so that a given cluster cannot contain voxels from different phases. The result of this

training stage is a unique identifier $I = 1 \dots k$ for each voxel of the DNS mesh. Voxels with same identifier have a similar microscopic response to macroscopic solicitations. Similarly to the convergence and sensitivity analysis that must be conducted when choosing an appropriate mesh for a FE simulation, the number of clusters k cannot be guessed *a priori* and requires a thorough analysis.

2.2.2 Prediction stage

As a result of the training stage, the RVE domain Ω^m is discretized into k subsets $(\Omega_I^m)_{I=1\dots k}$. The degrees of freedom in the FFT-based numerical method [14] are associated to the microscopic strain ε^m. In SCA [9], ε^m is discretized by a cluster-wise constant approximation $(\varepsilon_I^m)_{I=1\dots k}$. As a consequence, the microscopic Cauchy stress tensor is also approximated cluster-wise $(\sigma_I^m)_{I=1\dots k}$, and Eq. (2) can be discretized:

$$\varepsilon_I^m = -\sum_{J=1\dots k} D_{IJ}^0 : \left(\sigma_J^m - \mathrm{C}^0 : \varepsilon_J^m\right) + \varepsilon^0, I = 1 \dots k \tag{5}$$

where D^0 is the interaction tensor defined by

$$D_{IJ}^0 = \frac{1}{|\Omega_I^m|} \int_{\Omega^m} \chi_I^m(\mathrm{x}) \int_{\Omega^m} \chi_J^m(\mathrm{x}') \Phi^0(\mathrm{x}, \mathrm{x}') \mathrm{d}\mathrm{x}' \mathrm{d}\mathrm{x}. \tag{6}$$

The characteristic functions χ_I^m and χ_J^m are equal to 1 in, respectively, clusters I and J, and 0 elsewhere. In the FFT-based numerical method [14], the periodic Green's operator Φ^0 depends on C^0, and is known only in Fourier space. Because C^0 is associated to an isotropic linear elastic reference material, Φ^0 can be expressed in Fourier space as a function of the reference Lamé parameters λ^0 and μ^0. It is then obtained in real space by using the inverse FFT. In particular, Eq. (6) can be written in the form

$$\begin{aligned} D_{IJ}^0 &= f^1(\lambda^0, \mu^0) D_{IJ}^1 + f^2(\lambda^0, \mu^0) D_{IJ}^2, \\ D_{IJ}^i &= \frac{1}{|\Omega_I^m|} \int_{\Omega_I^m} \mathrm{FFT}^{-1} \left\{ \mathrm{FFT}\{\chi_J^m\} \hat{\Phi}^i \right\} (\mathrm{x}) \mathrm{d}\mathrm{x}, i = 1, 2. \end{aligned} \tag{7}$$

The detailed expressions of f^1, f^2, $\hat{\Phi}^1$ and $\hat{\Phi}^2$ can be found in Refs. [14, 8, 9] among others. Drastic computational cost reduction is enabled by SCA thanks to a reduced number of degrees of freedom by clustering, and by the fact that D^1 and D^2 can be precomputed in the training stage. Therefore, neither FFTs nor inverse FFTs are computed in the prediction stage, even if the reference material is changing.

In the present work, boundary conditions for Eq. (5) are purely kinematic. The average of the microscopic strain tensor ε^m must be enforced to be equal to the macroscopic strain tensor ε^M or, equivalently, the microscopic

fluctuation must have zero average. This can be done by adding the condition $\sum_{I=1...k} |\Omega_I^m|\varepsilon_I^m = |\Omega^m|\varepsilon^M$ to Eq. (5).

As noted in Ref. [9], solutions of Eq. 5 are dependent on the choice of reference material. An optimal choice can be computed in the prediction stage by making the reference material consistent with the homogenized material. This means that the far field strain tensor ε^0 is an additional unknown that must be solved for in SCA [9], as opposed to the FFT-based numerical method where $\varepsilon^0 \equiv \varepsilon^M$ [14]. The self-consistent method consists in using a fixed-point iterative method where, at each step, the reference Lamé parameters λ^0 and μ^0 are changed so that $||\sigma^M - \mathrm{C}^0 : \varepsilon^0||_2$ is minimized. A discussion on this self-consistent scheme and its mathematical foundations can be found in Ref. [17].

2.2.3 Summary

To summarize, the training stage in SCA consists in using a k-means clustering algorithm based on a mechanistic *a priori* clustering criterion computed using a simple sampling of the loading space. This training stage also includes computing all voxel-wise and computationally expensive operations such as FFTs and inverse FFTs.

In the prediction stage, a self-consistent iterative algorithm is used to search for the optimal choice of reference Lamé parameters. At each iteration of this self-consistent loop, matrix assembly operations are accelerated because all voxel-wise operations have been precomputed in the training stage and already reduced to cluster-wise contributions. In order to avoid recomputing the latter, clusters cannot be changed during the simulation. A Newton-Raphson iterative algorithm must be embedded within each self-consistent iteration for nonlinear materials, in which case the discrete Lippmann-Schwinger equation is linearized. The self-consistent nature of this algorithm is due to the fact that the reference Lamé parameters are iteratively corrected in order to be as close as possible to that of the homogenized material.

The output from SCA are the microscopic variables' cluster-wise approximations, and the macroscopic Cauchy stress tensor.

3 Multiscale damage

Concurrent computational homogenization implies introducing a macroscopic domain Ω^M, which can be a specimen or an industrial part. In the present work, the macroscale problem is solved using the FE method for the spatial discretization and an explicit scheme for the time discretization. The use of SCA as a material law is straightforward. Conventional constitutive equations

defining the macroscopic stress σ^M as a function of the macroscopic strain ε^M are replaced by the theory described in Sect. 2. Although macroscopic variables are constant in space at the microscale, they vary at the macroscale, namely, $\sigma^M = \sigma^M(\mathrm{x}), \varepsilon^M = \varepsilon^M(\mathrm{x}), \mathrm{x} \in \Omega^M$.

If the relation between macroscopic variables σ^M and ε^M included a softening effect, then the macroscale problem would be ill-defined. Softening would localize in a single arbitrary layer of elements, which would be dependent on the FE mesh, and lead to zero dissipated energy for very fine meshes. This well-known pathological mesh dependence problem when modeling softening materials can be solved by using non local integral averaging on the macroscopic damage variable [1]. The main issue in concurrent computational homogenization is that there is no macroscopic damage variable, since damage is modeled within RVEs. While Hill's lemma allows to formulate σ^M as the average σ^m, there is no such result for internal variables related to plasticity or damage.

As proposed in a recent work [10], non local integral averaging can be applied directly on the microscopic damage variable d^m. An additional difficulty when damage is modeled within the RVE, is that the RVE problem itself becomes ill-defined if damage localizes within the RVE. To avoid such situation, damage can be uncoupled from the microscale problem, and considered only in an average sense. These two steps are presented in the following. More details can be found in Ref. [10].

3.1 Macroscale damage

The damage variable d^m is defined at the microscale and discretized clusterwise along with the infinitesimal strain tensor and the Cauchy stress tensor. While these microscale variables have been written as functions of microscale coordinates in Sect. 2, they must now be written as functions of both macroscale and microscale coordinates.

First, a RVE domain $\Omega^m = \Omega^m(\mathrm{x}^M)$ is associated to each point x^M of the macroscale domain Ω^M. Since the macroscale problem is solved using the FE method, RVEs are attached to the integration points of the macroscale FE mesh.

Second, microscale variables can be written as functions of both macroscale and microscale coordinates, so that localization issues at microscale and macroscale can be distinguished and treated separately [10]. For instance, the microscale damage variable is discretized as

$$d^m(\mathrm{x}^M, \mathrm{x}^m) = \sum_{I=1\ldots k} d_I^m(\mathrm{x}^M)\chi_I^m(\mathrm{x}^M, \mathrm{x}^m), \mathrm{x}^M \in \Omega^M, \mathrm{x}^m \in \Omega^m(\mathrm{x}^M). \quad (8)$$

Third, classic non local integral regularization [1] can be applied to the microscale damage variable defined in Eq. (8), with the novelty that the averaging is applied at two scales [10]. The non local microscale damage variable $\overline{d}^m$ is hence defined by

$$\begin{aligned} \overline{d}^m(\mathrm{x}^M,\mathrm{x}^m) &= \sum_{I=1\ldots k} \overline{d}^m_I(\mathrm{x}^M)\chi^m_I(\mathrm{x}^M,\mathrm{x}^m), \mathrm{x}^M \in \Omega^M, \mathrm{x}^m \in \Omega^m(\mathrm{x}^M), \\ \overline{d}^m_I(\mathrm{x}^M) &= \int_{\Omega^M} w(||\mathrm{x}^M - \mathrm{y}^M||_2) d^m_I(\mathrm{y}^M)\mathrm{d}\mathrm{y}^M, \mathrm{x}^M \in \Omega^M, \end{aligned} \tag{9}$$

where w is the non local averaging kernel given by

$$\begin{aligned} w(r) &= \frac{w_\infty(r)}{\int_0^{+\infty} w_\infty(r')\mathrm{d}r'}, r \in [0,+\infty[, \\ w_\infty(r) &= \begin{cases} \left(1 - 4\dfrac{r^2}{l_c^2}\right)^2, & r \le l_c \\ 0, & r > l_c \end{cases}, r \in [0,+\infty[. \end{aligned} \tag{10}$$

The characteristic length scale l_c is a material parameter associated to the width of damage localization bands at the macroscale. As defined by Eqs. (9) and (10), the non local damage variable is regularized at the macroscale and the macroscale FE problem is hence well-defined. In particular, results will not pathologically depend on the macroscale FE mesh. However, the non local damage variable may still localize at the microscale and yield clustering-dependent results.

3.2 Microscale damage

To prevent localization within RVEs, an averaging procedure is also applied at the microscale. This procedure consists in uncoupling the damage model from the plasticity model, and modeling softening only in an average sense.

First, the microscopic infinitesimal strain tensor ε^m is additively decomposed into an elastic part $\varepsilon^{m,el}$ and a plastic part $\varepsilon^{m,pl}$. The microscopic damage variable d^m is written as a function of the plastic strain $d^m = d^m(\varepsilon^{m,pl})$, but the plastic strain itself is not a function of the damage variable. Eq. (5) is hence solved with a first definition of the microscopic Cauchy stress tensor that does not account for softening.

Second, the evolution of the damage variable is computed based on the stress state and plastic strain computed in the first step. For the CFRP composite studied in Sect. 4, the following power law is used to define the evolution of damage in the epoxy matrix as a function of the von Mises equivalent plastic strain $\varepsilon^{m,pl,eq}$:

$$d^{epoxy} = 1 - \frac{\varepsilon^{m,pl,c}}{\varepsilon^{m,pl,eq}} \exp\left(-100(\varepsilon^{m,pl,eq} - \varepsilon^{m,pl,c})\right) \tag{11}$$

This law involves the material parameter $\varepsilon^{m,pl,c} = 0.13$. The brittle fracture of fibers is modeled by maximum stress theory [2]. Thus, the damage variable in fibers can be equal only to 0 or 1.

Third, the effective macroscopic Cauchy stress tensor σ^M is computed by solving Eq. (5) with a softening effect but no plasticity, namely, C^m being the microscopic elastic stiffness tensor, $\sigma^m = (1 - \overline{d}^m)C^m : \varepsilon^{m,el}$. The applied macroscopic strain for this third step is the macroscopic elastic strain computed by elastic relaxation and averaging of the first step solution [10].

Although this averaging procedure requires two solutions of Eq. (5), only the first one accounts for plasticity and material nonlinearity. Thus, the second solution has a reduced cost. Furthermore, both solutions are accelerated thanks to SCA.

Because the microscopic plastic strain does not depend on damage, it can not localize pathologically within a single layer of clusters. Then, the damage variable being written as a function of the microscopic plastic strain, pathological localization of this variable is not possible within the RVE. With the addition of the macroscale non local integral averaging described in Sect. 3.1 that prevents pathological localization and mesh dependence at the macroscale scheme, a regularized multiscale damage theory is obtained.

4 Multiscale carbon fiber reinforced polymer composite cutting process modeling

An example of concurrent simulation of the cutting process of a UD CFRP composite is proposed in this section. Literature reports some progress made in simulating CFRP cutting processes at the microscale [2, 6]. This is necessary to observe microscale deformation, such as fiber distortion and matrix cracking during this process. For a full scale cutting process, the material is generally assumed homogeneous and modeled using phenomenological constitutive equations to reduce the computational cost, but all microscale details are lost. The theory presented in this paper opens a new window for structure scale simulation with minimum loss of microscale details.

The cutting simulation is based on experimental work performed in a previous study [2]. The key difference between the model presented here and Ref. [2] is that here all fibers are implicitly modeled as clusters. This allows modeling of a larger UD CFRP part with width of 0.2 mm. Details of the experimental setup can be found in the given reference. To demonstrate the capabilities of the multiscale modeling theory presented in this paper, a 3D transverse UD CFRP cutting simulation is performed on a domain of

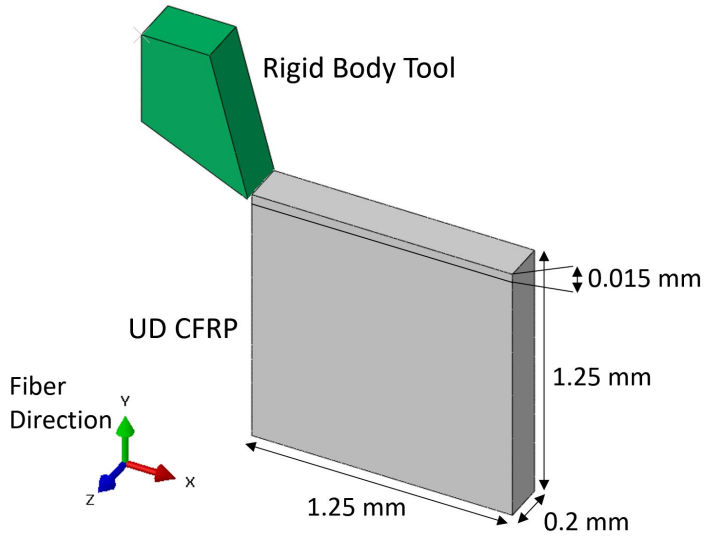

Fig. 2 Cutting simulation setup and geometry of UD CFRP part

length x weight x height of 1.25mm x 0.2mm x 1.25mm. The cutting depth is 0.015mm, following the experimental setup. The model setup is shown in Fig. 2. The bottom surface of the UD CFRP part is fixed to ensure that it stays in its position. Cutting speed is set to 8mm/s according to the experimental setup. The UD CFRP part is modeled with 142,500 reduced integration cubic elements, where each element has one integration point.

The UD CFRP material has fiber volume fraction of 60%. Fiber is assumed to be of circular shape with a diameter of 7 μm, as shown in Fig. 3a. The RVE has an identical length and width of 84 μm, and a depth of 14 μm. The RVE is meshed with 740x740x5 voxels, which are then clustered using the method presented in Sect. 2.2.1 into 16 clusters for the matrix, and 16 additional clusters for the fibers. As shown in Ref. [9], 16 clusters in each phase are sufficient to preserve the accuracy of the RVE solution. This choice is also efficient due to the saving regarding the total number of degrees of freedom. The result is shown in Fig. 3b.

Fiber and matrix elastic properties are given in Tab. 1. Fibers tensile and compressive strengths follow the parameters listed in Ref. [2]. It is assumed that excessive deformation of the matrix happens when the cutting tool is in compressive contact with the material. Thus, matrix plasticity has been calibrated to the uniaxial compression curve for epoxy in Fig. 1 of Ref. [13] with a simple J_2 plasticity model. The damage evolution law for the matrix has been given in Eq. (11).

Using the damage evolution law in Eq. (11) within the multiscale damage modeling theory, the microscale damage variable might reach 1 in some clusters. In such case, the material has completely lost its load carrying capacity. If

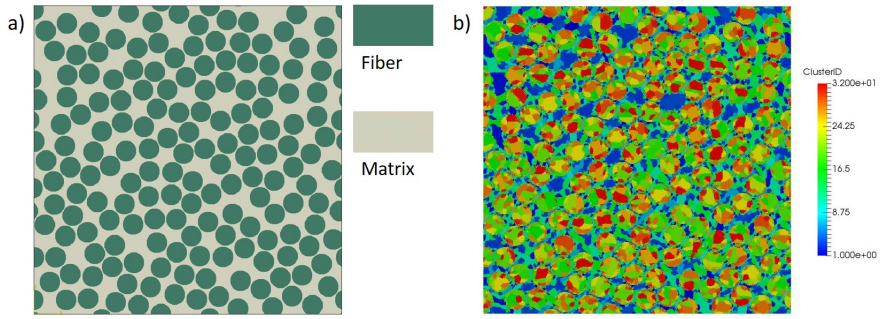

Fig. 3 Cross section of the UD CFRP RVE showing: (a) the random fibers arrangement; (b) the clusters

Table 1 Carbon fiber and epoxy matrix elastic properties

E_1	E_2	E_3	v_{12}	v_{13}	v_{23}	E_m	v_m
240 GPa	19 GPa	19 GPa	0.28	0.28	0.32	3.8 GPa	0.387

this happens for multiple clusters, the averaged load carrying capacity of some RVEs might be significantly lost. With a criterion to measure this loss of averaged load carrying capacity, element deletion could be triggered in the macroscale mesh to model the cutting process. A macroscopic non local damage variable $\overline{d}^M$ is introduced to measure this loss of averaged load carrying capacity:

$$\overline{d}^M = 1 - \frac{||\sigma^M : \sigma_{pl}^M||}{||\sigma_{pl}^M : \sigma_{pl}^M||} \tag{12}$$

where σ_{pl}^M is the average of the Cauchy stress tensor computed with the plasticity model but no damage, while σ^M is the macroscopic Cauchy stress tensor computed with the non local damage model but no plasticity. For each element of the UD CFRP part FE model, element deletion is triggered when $\overline{d}^M = 0.25$.

Simulation of concurrent UD CFRP cutting has been performed for 0.01s using ABAQUS CAE with the multiscale damage model. The average reaction force obtained from concurrent cutting was 0.881 N. The comparison between numerical result and experimental result is presented in Tab. 2. The simulated average horizontal cutting force is 7.3% less than that measured in the experiment.

Table 2 Comparison of simulated cutting force against experimental data

	Experimental data [2]	Multiscale model	Difference
Horizontal cutting force	0.946 N/m	0.881 N/m	7.3%

The main feature of the multiscale model is that it captures the microscale fiber and matrix failure within UD RVEs at each integration point of the macroscale part. Fig. 4 shows the macroscopic part with RVEs at three selected integration points where damage can be seen at different phases of the cutting process. At different time steps, it can be seen that different elements have different macroscopic non local damage $\overline{d}^M$ that can be traced back to the microscopic damage d^m within each cluster in RVEs. Here, the element embedding the second RVE fails after the element embedding the first RVE, although it seems to have a higher total damaged volume. This shows the effect of the element deletion criterion in Eq. (12), which does not define the macroscopic damage variable just as the average of the microscopic one, but as the actual loss of load carrying capacity. Additionally, the local damage within damaged elements RVEs is transferred to neighboring elements RVEs via non local averaging. This can be seen from the left column of Fig. 4, where localized damage is being distributed to nearby elements from those contacting the tool. As a consequence, some damage can be seen in the third RVE, but it does not cause enough loss of load carrying capacity for the associated element to get deleted.

5 Conclusions

Two main contributions were presented in this paper. A regularized multiscale modeling theory was proposed to model multiscale damage and fracture processes such as the fracture of material systems with heterogeneous microstructure. The latter was modeled using the self-consistent clustering analysis method for data-driven reduced order modeling.

To illustrate the capabilities of this data-driven multiscale damage and fracture modeling theory, a simulation of a cutting process was conducted. The considered material, a carbon fiber reinforced composite, exhibited a heterogeneous microstructure which failed by epoxy matrix damage and fiber breakage. The effect of these microscale damage and fracture mechanisms on the macroscale behavior was modeled using a material law computed on-the-fly by the multiscale modeling theory instead of relying on conventional phenomenological constitutive equations.

For future work, the proposed theory is going to be extended to other material and processes involving more complex damage and fracture mechanisms.

Acknowledgements All the authors warmly thank the support from National Institute of Standards and Technology and Center for Hierarchical Materials Design (CHiMaD) under grant No. 70NANB13Hl94 and 70NANB14H012, and DOECF-ICME project under grant No. DE-EE0006867. WKL is also thankful to the National Science Foundation (NSF) Mechanics of Materials and Structures (MOMS) for support under the newly funded grant No. MOMS/CMMI-1762035.

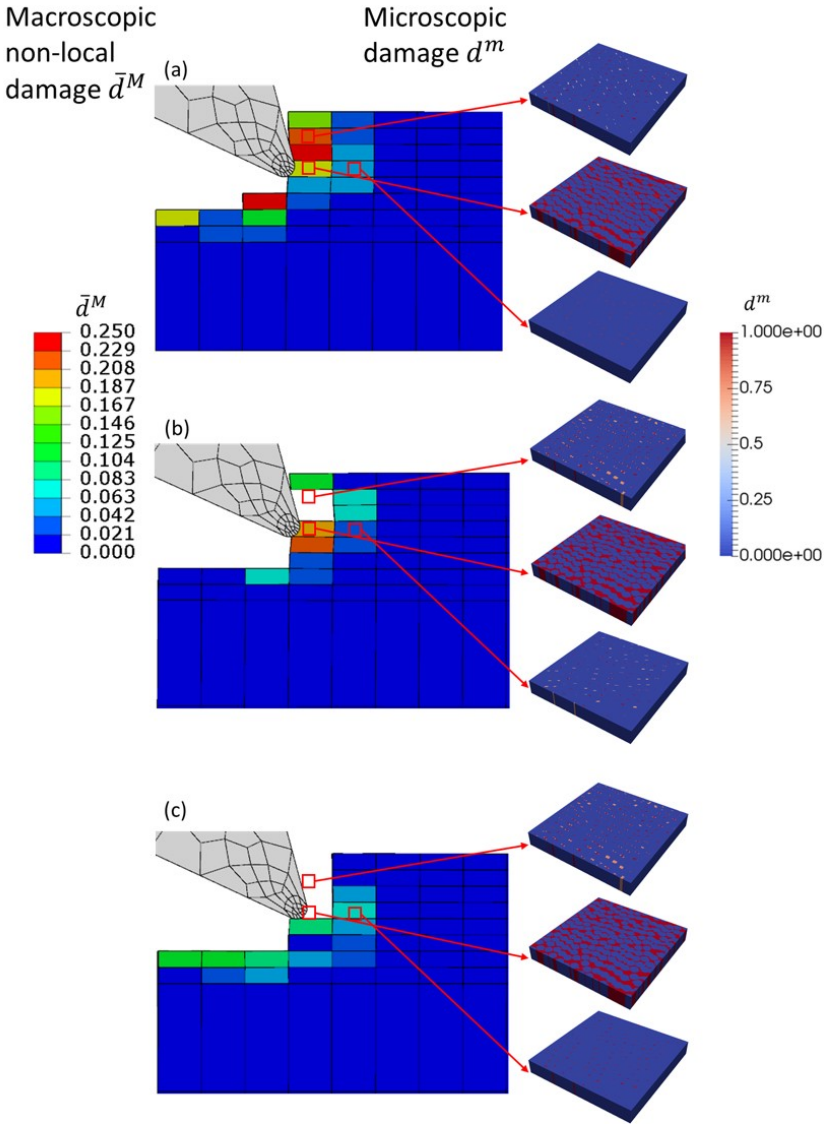

Fig. 4 Macroscopic non local damage variable and microscopic damage variable at: (a) 5.125e-3 s; (b) 5.250e-3 s; (c)5.5e-3 s

References

1. Zdeněk P. Bažant and Milan Jirásek, *Nonlocal Integral Formulations of Plasticity and Damage: Survey of Progress*, Journal of Engineering Mechanics **128** (2002), no. 11, 1119–1149.

2. Hui Cheng, Jiaying Gao, Orion Landauer Kafka, Kaifu Zhang, Bin Luo, and Wing Kam Liu, *A micro-scale cutting model for ud cfrp composites with thermo-mechanical coupling*, Composites Science and Technology **153** (2017), 18–31.
3. F. Chinesta, A. Leygue, F. Bordeu, J. V. Aguado, E. Cueto, D. Gonzalez, I. Alfaro, A. Ammar, and A. Huerta, *PGD-Based Computational Vademecum for Efficient Design, Optimization and Control*, Archives of Computational Methods in Engineering **20** (2013), no. 1, 31–59.
4. Olivier Goury, David Amsallem, Stéphane Pierre Alain Bordas, Wing Kam Liu, and Pierre Kerfriden, *Automatised selection of load paths to construct reduced-order models in computational damage micromechanics: from dissipation-driven random selection to Bayesian optimization*, Computational Mechanics **58** (2016), no. 2, 213–234.
5. J.A. Hernández, J Oliver, A E Huespe, M A Caicedo, and J C Cante, *High-performance model reduction techniques in computational multiscale homogenization*, Computer Methods in Applied Mechanics and Engineering **276** (2014), 149–189.
6. D. Iliescu, D. Gehin, I. Iordanoff, F. Girot, and M.E. Gutiérrez, *A discrete element method for the simulation of cfrp cutting*, Composites Science and Technology **70** (2010), no. 1, 73 – 80.
7. William J. Joost, *Reducing Vehicle Weight and Improving U.S. Energy Efficiency Using Integrated Computational Materials Engineering*, JOM **64** (2012), no. 9, 1032–1038.
8. Matthias Kabel, Thomas Böhlke, and Matti Schneider, *Efficient fixed point and Newton–Krylov solvers for FFT-based homogenization of elasticity at large deformations*, Computational Mechanics **54** (2014), no. 6, 1497–1514.
9. Zeliang Liu, M.A. Bessa, and Wing Kam Liu, *Self-consistent clustering analysis: An efficient multi-scale scheme for inelastic heterogeneous materials*, Computer Methods in Applied Mechanics and Engineering **306** (2016), 319–341.
10. Zeliang Liu, Mark Fleming, and Wing Kam Liu, *Microstructural material database for self-consistent clustering analysis of elastoplastic strain softening materials*, Computer Methods in Applied Mechanics and Engineering **330** (2018), 547–577.
11. J Macqueen, *Some methods for classification and analysis of multivariate observations*, Proceedings of the Fifth Berkeley Symposium on Mathematical Statistics and Probability **1** (1967), no. 233, 281–297.
12. Karel Matouš, Marc G.D. Geers, Varvara G Kouznetsova, and Andrew Gillman, *A review of predictive nonlinear theories for multiscale modeling of heterogeneous materials*, Journal of Computational Physics **330** (2017), 192–220.
13. AR Melro, PP Camanho, FM Andrade Pires, and ST Pinho, *Micromechanical analysis of polymer composites reinforced by unidirectional fibres: Part i–constitutive modelling*, International Journal of Solids and Structures **50** (2013), no. 11, 1897–1905.
14. H Moulinec and P Suquet, *A numerical method for computing the overall response of nonlinear composites with complex microstructure*, Computer Methods in Applied Mechanics and Engineering **157** (1998), no. 1-2, 69–94.
15. Jitesh H. Panchal, Surya R. Kalidindi, and David L. McDowell, *Key computational modeling issues in Integrated Computational Materials Engineering*, Computer-Aided Design **45** (2013), no. 1, 4–25.
16. Jacob Smith, Wei Xiong, Wentao Yan, Stephen Lin, Puikei Cheng, Orion L. Kafka, Gregory J. Wagner, Jian Cao, and Wing Kam Liu, *Linking process, structure, property, and performance for metal-based additive manufacturing: computational approaches with experimental support*, Computational Mechanics **57** (2016), no. 4, 583–610.
17. Shaoqiang Tang, Lei Zhang, and Wing Kam Liu, *From virtual clustering analysis to self-consistent clustering analysis: a mathematical study*, Computational Mechanics **in press** (2018).